



Diclofenac sodium adsorption in aqueous media by activated carbon obtained from einkorn (*Triticum monococcum L.*) husk

Barış Kocabıyık¹ · Osman Üner² · Ünal Geçgel³

Received: 29 February 2024 / Revised: 19 April 2024 / Accepted: 22 April 2024 / Published online: 9 May 2024
© The Author(s) 2024

Abstract

The uncontrolled release of waste diclofenac with low biodegradability is considered to be a potential threat for the environment and creatures. To find effective solution for this issue, this study reports the adsorption performance of diclofenac sodium salt (DCF) by using activated carbon (EHAC) obtained from einkorn (*Triticum monococcum L.*) husk in aqueous solution under various circumstances. It was found that DCF adsorption on EHAC was highly solution pH dependent, and DCF adsorption by EHAC decreased with increasing adsorption temperature. Equilibrium data showed that fitted isotherm model with the experiment results of DCF adsorption on EHAC followed the order of Langmuir > Temkin > Freundlich > Dubinin-Radushkevich. Adsorption capacity of EHAC for DCF adsorption in aqueous solution was calculated to be 147.06 mg/g at 25 °C. The adsorption kinetic of DCF adsorption on EHAC was determined to obey the pseudo-second-order kinetic model. By utilizing FTIR and pH data obtained from DCF adsorption on EHAC, DCF adsorption mechanisms with some interactions such as π - π stacking, electrostatic interactions, and hydrogen bonding were suggested at diverse pH values. Additionally, intraparticle diffusion model was applied to kinetic results to further recognize the kinetic mechanism of DCF adsorption on EHAC. Furthermore, thermodynamic parameters for DCF adsorption on EHAC were calculated and evaluated, in which DCF adsorption process by EHAC was determined to be exothermic, spontaneous, and feasible.

Keywords Diclofenac sodium adsorption · Einkorn husk activated carbon · Mechanism · Water treatment

1 Introduction

All over world, non-steroidal anti-inflammatory drugs (NSAIDs) have been extensively utilized in pharmaceutical industry but listed in emerging pollutant catalogue because of their adverse effects on the human health and environment [1–6]. One of NSAIDs is sodium diclofenac (DCF), which is o-(2,6-dichlorophenylamino)-phenyl acetic acid sodium salt [5, 7, 8]. Potassium diclofenac also is the other

salt form of diclofenac [9]. To decrease inflammation and relieve pain in arthritis and acute injuries, diclofenac is used such as in osteoarthritis, ankylosing spondylitis, and rheumatoid arthritis [10, 11]. It was predicted that 940 tons of diclofenac were consumed yearly worldwide [12], but it has ranked 13th among the best-selling generic drugs recently and reported its yearly consumption between 195 and 940 mg per person in various countries [13].

The unusual pain reliever potential of DCF leads to its overuse to cure pain; therefore, this results in its unmonitored release in water flows [14]. The releases of diclofenac emerge from the urine with its active metabolisms, unsuitable disposal as solid waste, pharmaceutical units, hospital effluents, domestic wastes, wastewaters from urban and industrial wastewater treatment factories [14, 15]. Diclofenac enters surface waters from wastewater treatment plants after treatment, and it is mainly detected in freshwater bodies [16]. Many studies have been implemented for potentially deleterious effects of diclofenac on aquatic environment

✉ Osman Üner
osmanuner@klu.edu.tr

¹ Department of Textile, Clothing, Shoes and Leather, Vocational College of Technical Sciences, Tekirdağ Namık Kemal University, 59030 Tekirdağ, Türkiye

² Department of Chemistry, Science and Art Faculty, Kırklareli University, 39020 Kırklareli, Türkiye

³ Arda Vocational College, Trakya University, 22030 Edirne, Türkiye

[17–22]. Diclofenac with low biodegradability is considered as a high-risk molecule in water bodies [22].

There are various studies to assess the risky effects of diclofenac in marine species; in which these species have diverse sensitivities to diclofenac, depending on exposure time and variety of species, but the more studies are needed to evaluate the unknown potential risks on marine species [23]. The uncontrolled release of waste diclofenac may have potential adverse effects not only for aquatic species but also for human beings directly by drinking tap water and indirectly by eating diclofenac exposure species. In various countries, such as, Spain, Sweden, Japan, and France, diclofenac was detected in drinking water [24]. Other than these, waste diclofenac may have hazardous effects in soil-related environmental compartments and biota. Diclofenac was detected in the surface soil at irrigated areas and around treatment factories in various countries, such as Spain [25] and Pakistan [26]. Thus, the long-term presence of diclofenac in water bodies should be reduced and removed by appropriate methods.

The determination of appropriate techniques is crucial to develop efficient process for diclofenac removal from aqueous solution. There are various water treatment techniques; physical processes: such as reverse osmosis [27], adsorption [28], and membrane filtration [29], chemical processes: such as ion exchange [29], chemical precipitation [29, 30], coagulation-flocculation [31], electrocoagulation [32], biological processes: such as activated sludge [33] and anaerobic process [34]. These techniques possess their own disadvantages and advantages in terms of cost, applicability, efficiency, simplicity, toxic byproducts, operability, environmental effect, and other factors [35, 36].

One of the most widely applied techniques for efficient pollutant removal from aqueous solution is adsorption because of low cost, simple operation, environmental-friendly, and high efficiency [37–42]. At the adsorption processes for pollutant removals from aqueous solutions, activated carbon is extensively utilized as an adsorbent owing to its great surface area, adjustable porous structure, various functional groups, and strong adsorption capacity [43, 44]. Also, diverse chemical activating reagents such as H_3PO_4 , NaOH, KOH, and $ZnCl_2$ are used to improve the surface properties and the porous structures of activated carbons [43]. In recent years, waste biomasses such as ripe black locust seed pods [27], soybean oil cake [45], waste tea [46], sugarcane bagasse [47], orange peels [48], walnut shell [49], etc. have been taken great attention as raw materials to obtain activated carbons. Einkorn (*T. monococcum* L.) is one kind of cereals whose cultivation was started by ancient people in southeastern Türkiye 10,000–12,000 years ago [50]. There is a rising interest in einkorn cultivation due to its nutritionally rich content, such as protein, carotenoid,

tocol, lipid, mineral, etc., and resistance to diseases [51, 52]. Before einkorn is milled to flour for consumption, it is necessary to dehusk the grain. Husks account for almost half of the harvest by weight, and their usage areas are limited. Therefore, it would be appropriate to use a starting material of activated carbon for adsorption processes.

The aim of this study was to evaluate the adsorption performance of diclofenac sodium by activated carbon (EHAC) obtained from einkorn (*Triticum monococcum* L.) husk. The factors, affecting adsorption performance, such as pH, contact time, initial dye concentration, and adsorbent dosage were analyzed with data obtained from batch adsorption experiments. Based on the experimental data, kinetic studies, adsorption isotherms, and thermodynamic studies were carried out. In addition, the adsorption mechanism of DCF at various pH values on activated carbon obtained from einkorn husk was explained by utilizing FTIR and pH data.

2 Materials and methods

2.1 Materials

Einkorn husk used was obtained from central Anatolia region in Türkiye. DCF ($C_{14}H_{10}Cl_2NNaO_2$, purity $\geq 98\%$, 318.13 g/mol) and $ZnCl_2$ were supplied by Merck. HCl (37 wt%), KNO_3 , and KOH were acquired from Sigma-Aldrich. All reagents used are analytical grade.

2.2 Preparation of adsorbent

As described in the paper [53], activated carbon was prepared from einkorn (*Triticum monococcum* L.) husk with starting material/ $ZnCl_2$ ratio of 1/2 at 500 °C for an hour. Briefly, 10 g dried einkorn husks and 50 ml $ZnCl_2$ solution (20 g) were mixed, heated under reflux for an hour at boiling temperature. Then, the mixture was waited in an incubator (Binder ED 115) at 105 °C for 24 h. By using a crucible with lid, dried mixture was carbonized in a muffle furnace (Daihan Scientific FX-14) at 500 °C for an hour. After that, EHAC obtained was treated with 0.1 N HCl, washed with distilled water, and dried in the incubator at 60 °C.

2.3 Batch adsorption experiments

By utilizing Batch sorption technique [54], DCF adsorption experiments by EHAC were executed in a series of 100 mL glass Erlenmeyer flasks with lids. 1 g/L stock solution of DCF was used for the preparation of 10–50 mg/L DCF solutions by doing dilution with double-distilled water. By preparing EHAC concentrations from 2.5–30 mg/50mL, adsorbent dosage effect was studied in various DCF concentrations

(10–50 mg/L). Each prepared solutions with the desired concentrations of EHAC and DCF were placed into a shaking water bath with temperature control (WiseBath). To mix EHAC with DCF, these solutions were shaken at 160 rpm under 25 °C till reaching adsorption equilibrium. Then, they were centrifuged in a centrifugal instrument (LC-04 A) for 15 min at 4000 rpm to separate supernatants from EHAC. The DCF amounts adsorbed by EHAC in supernatant solutions were determined spectrophotometrically using UV-vis spectrophotometer (Mecasys Optizen POP Series) at 272 nm. All measurements in adsorption experiments were repeated at least three times, and the presented results are given as the average value.

The experiments performed to investigate the initial DCF concentration, and the effect of were done at 25, 35, and 45 °C by holding EHAC concentration at constant value (15 mg/50L).

The percentage of removal efficiency and the amount of DCF adsorbed by EHAC, q_e (mg/g), were calculated by using following equations [55].

$$\text{Removal efficiency (\%)} = \frac{(C_0 - C_e)}{C_0} \times 100 \tag{1}$$

$$q_e = \frac{(C_0 - C_e)}{w} \times V \tag{2}$$

where q_e (mg/g) is the amount of DCF adsorbed at equilibrium. q_t (mg/g) is the amount of adsorption at time t . C_0 symbolizes the initial DCF concentration (mg/L) while C_e is DCF equilibrium concentration (mg/L). Also, V is solution volume (L), and w is EHAC mass (g).

Also, the experiments performed to investigate the contact time at their original pHs were carried out by

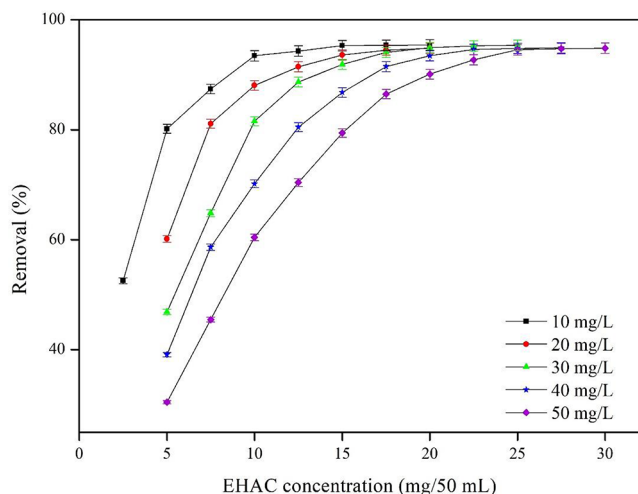


Fig. 1 Effect of adsorbent dosage on DCF adsorption under conditions: where DCF solution volume = 50 mL, agitation speed = 160 rpm, temperature = 25 °C, contact time = 180 min, and pH value = original

utilizing various initial DCF concentrations of 10 – 50 mg/L at 25 °C by holding AHCS concentration at constant value (15 mg/50L) for 180 min.

A benchtop pH meter (Orion Star™ A211) and Fourier transform infrared spectrometer (Bruker Vertex 70) were used for the characterization of adsorption mechanism. According to the procedure [56], the point of zero charge of EHAC had been measured in the recently published paper [53]. Briefly, 0.1 N 50 mL KNO₃ solutions were prepared in each Erlenmeyer flask with lid, and their pH values were set from 2 to 12 by utilizing 0.1 N solutions of HCl or NaOH. 0.1 g EHAC was added into each one, and these were stirred at 150 rpm for 48 h. Then, the final pH values were measured to graph with the initial pH values.

3 Results and discussion

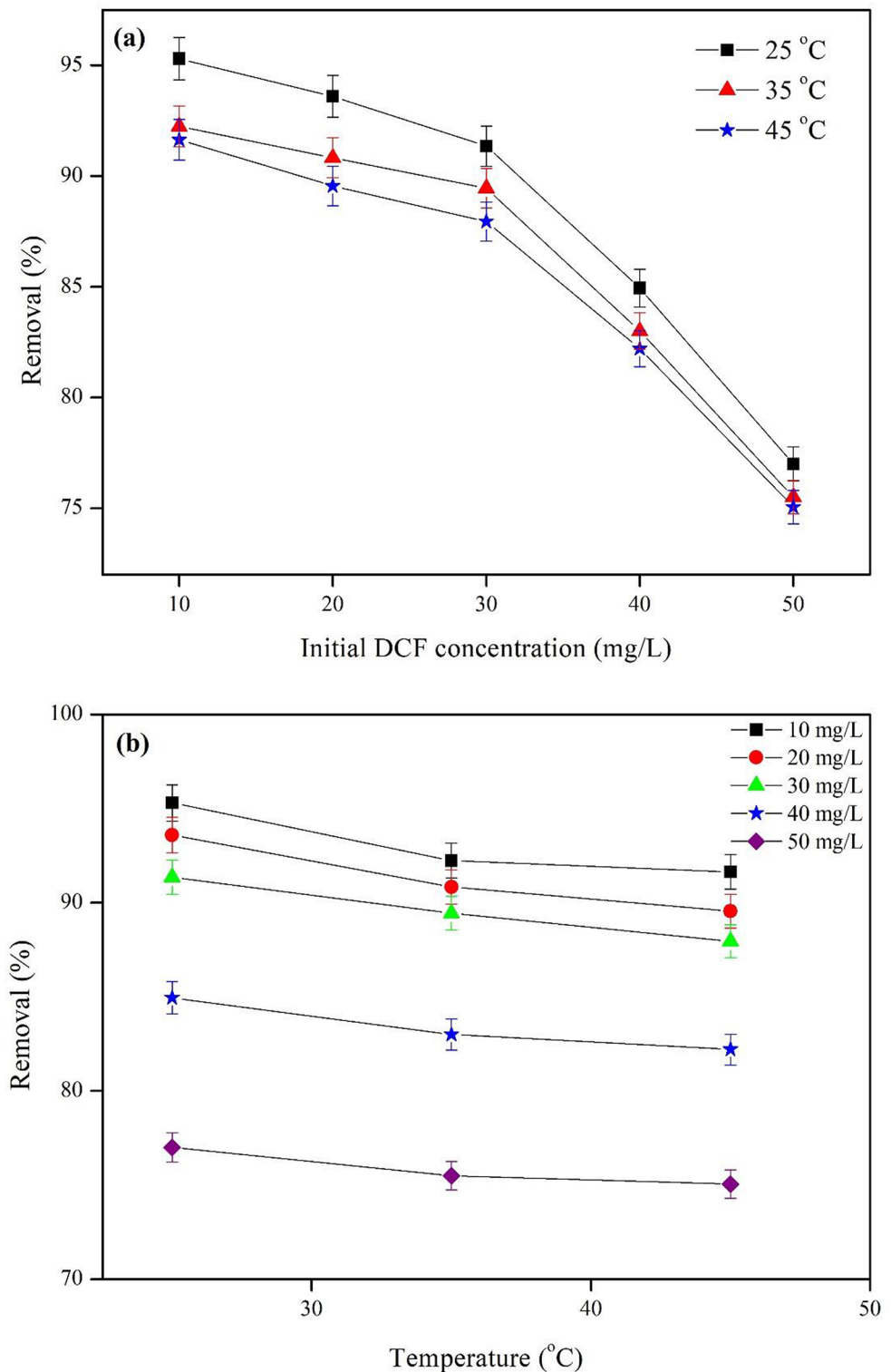
3.1 Effect of adsorbent dosage

EHAC dosage was varied from 2.5 to 30 mg/50mL for various DCF concentrations from 10 to 50 mg/L. The adsorbent dosage effect on DCF removal efficiency by EHAC at 25 °C is presented in Fig. 1. As expected, DCF removal percentage is increased with increasing EHAC dosage owing to the increase in surface area of EHAC, which provides more available EHAC surface area for free DCF ions in solution. The percentages of DCF removal are not changed significantly after EHAC dosage values of 15, 17.5, 20, 22.5, and 25 mg/50 mL respectively for 10 through 50 mg/L DCF concentrations, because the amounts of DCF decrease excessively in solution. Also, as seen in Fig. 1, the separate applications of 15, 17.5, 20, 22.5, and 25 mg/50 mL EHAC dosages resulted in 95.30%, 94.50%, 94.93%, 94.61%, and 94.55% DCF removals respectively for 10 through 50 mg/L DCF solutions.

3.2 Effect of initial DCF concentration and adsorption temperature

By varying the initial DCF concentration and adsorption temperature, their influences on DCF adsorption performance on EHAC was studied by holding EHAC dosage concentration at constant value of 15 mg/50mL as depicted in Fig. 2. As expected, in Fig. 2(a), the percentage of DCF removal from the solution by EHAC decreases for all temperatures when the initial DCF concentration increases in the solution. This is because the amount of EHAC is kept constant (15 mg/50mL), and the EHAC surface covered by DCF ions after saturation cannot find a binding surface for the free DCF ions remaining in the solution. While DCF removal percentages on adsorption equilibrium are between

Fig. 2 Effect of (a) initial DCF concentration and (b) adsorption temperature under conditions: where EHAC dosage = 15 mg/50mL, DCF solution volume = 50 mL, agitation speed = 160 rpm, contact time = 180 min, and pH value = original



91.64 and 95.30 at all studied temperatures, they decrease to 75.05% and 77.00% when initial DCF concentration increases from 10 mg/L to 50 mg/L.

Figure 2(b) displays the effect of temperature on DCF adsorption by EHAC for various initial concentration values of 10–50 mg/L. When 10 mg/L initial DCF concentration

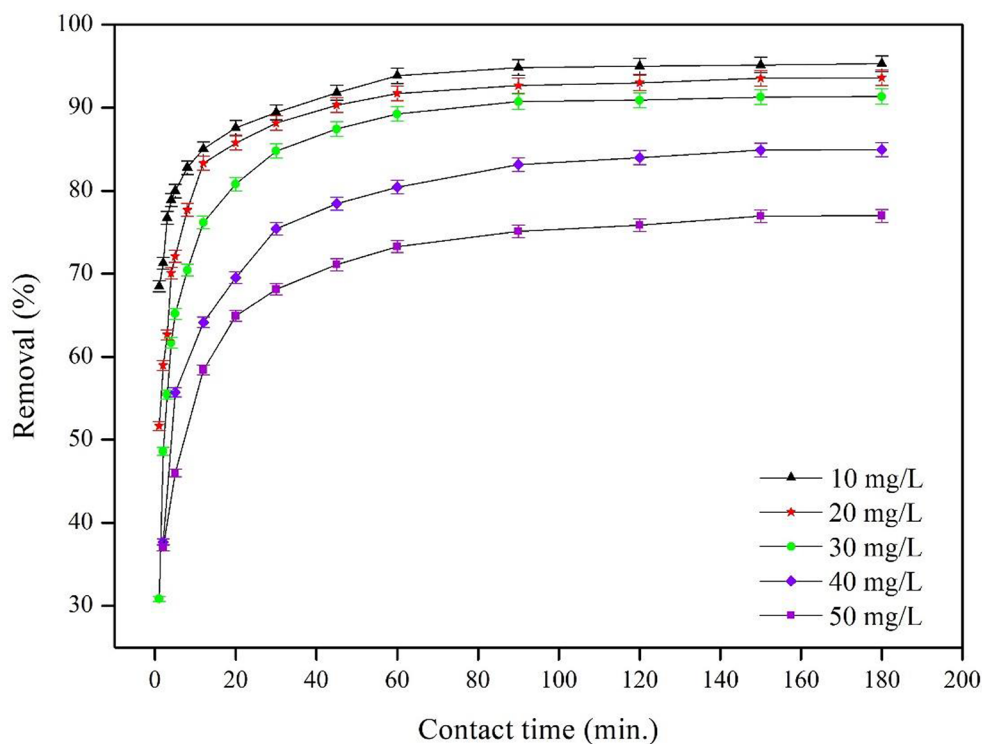
is used, the DCF removal percentage reduces from 95.30 to 91.64 with increasing temperature from 25 to 45 °C. The same trends are seen for the other initial DCF concentrations studied. Namely, decrease in temperature favors the DCF adsorption process with EHAC, indicating exothermic nature of DCF adsorption on EHAC. Decrease in DCF

adsorption with temperature increase may be due to higher Brownian movements of molecules, causing bond weakening between DCF ions and EHAC functional groups, and also higher temperature may bring about the breakings of intermolecular hydrogen bonds [57].

3.3 Effect of contact time

By utilizing various initial DCF concentrations of 10–50 mg/L at 25 °C adsorption temperature, the effect of contact time on DCF adsorption by EHAC is illustrated in Fig. 3 at times between 0 and 180 min. The extent of DCF removal by EHAC increased when contact time increase for all initial DCF concentrations. DCF adsorptions by EHAC for all initial DCF concentrations used are rapid in contact time of 12 min. and then slow down with increasing contact time until reaching adsorption equilibriums. This phenomenon could be explained with high availability of vacant accessible sites on EHAC for DCF ions at initial periods of contact time, and after that, progressively occupations of DCF ions on EHAC until the adsorption equilibriums [55]. In Fig. 3, DCF removal percentages by EHAC were determined to be 85.02, 83.31, 76.18, 64.15, and 58.42 at 12th minute respectively for 10 through 50 mg/L initial DCF concentrations, while 95.30, 93.60, 91.35, 84.95, and 77.00 at adsorption equilibrium of 180th minute.

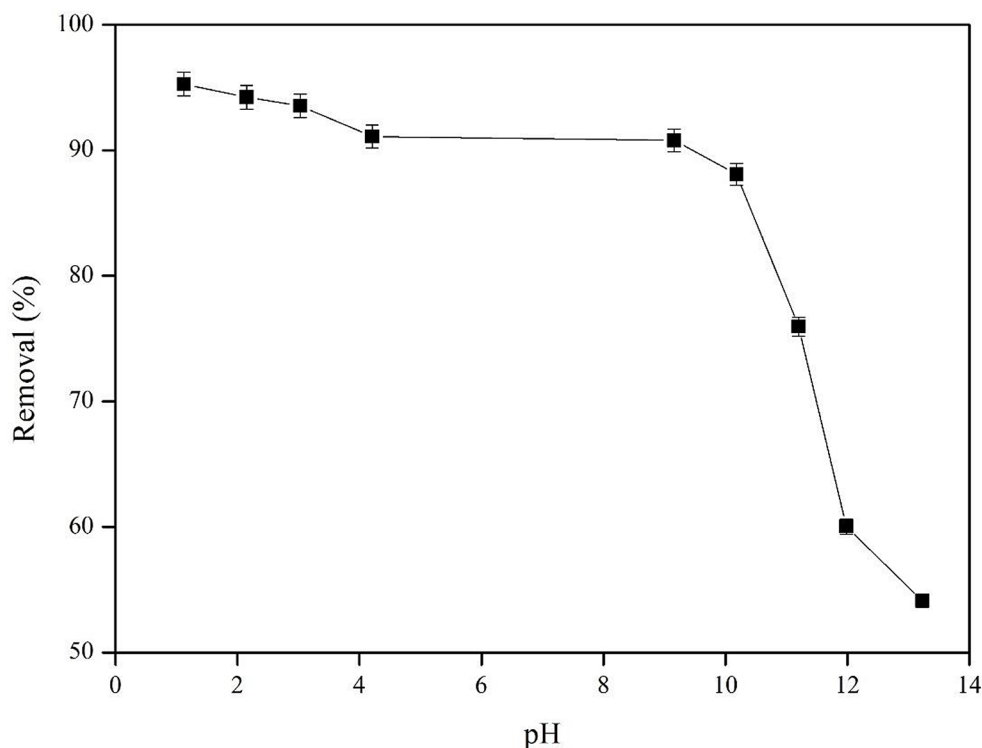
Fig. 3 Effect of contact time under conditions: where EHAC dosage = 15 mg/50mL, DCF solution volume = 50 mL, temperature = 25 °C, agitation speed = 160 rpm, and pH value = original



3.4 Effect of adsorption pH

Effect of pH on DCF adsorption on EHAC was studied by adjusting the pH values of solutions between 1.12 and 13.23 because pH value has significant effects on adsorption processes. By holding initial DCF concentration (20 mg/L) and EHAC dosage (12.5 mg/50mL) at constant values, pH values were measured with a benchtop pH meter at 25 °C. Figure 4 presents pH effect on DCF adsorption by EHAC under its set conditions. When the pH is increased from 1.12 to 4.21, it is seen a small decrease in the removal percentage of DCF by EHAC from 95.27 to 91.10%. The point of zero charge of EHAC had been determined to be 7.33 as measured in the paper [53]. Below this pH of 7.33, EHAC surface is positively charged. Also, the pKa value of DCF is around 4.20, therefore DCF is at unionized form below 4.20 and is negatively charged above 4.20 because of its ionization [58]. It is obvious that the attractions between positively charged EHAC and DCF molecules with unionized form at lower pH values (below 4.20) are stronger than those between negatively charged EHAC and negatively charged DCF ions at higher pH values (above 7.33). Therefore, the removal percentage of DCF by EHAC is reduced more at higher pH values. When the pH is increased from 4.21 to 9.16, the removal percentage of DCF by EHAC decreases from 91.10 to 90.80%. When pH value increases from 9.16 to 13.23, the removal percentage of DCF by EHAC decreases significantly from 90.80 to 54.12%.

Fig. 4 Effect of solution pH on DCF adsorption under conditions: where EHAC dosage = 12.5 mg/50mL, initial DCF concentration = 20 mg/L, DCF solution volume = 50 mL, agitation speed = 160 rpm, temperature = 25 °C, and contact time = 180 min



3.5 Adsorption isotherms

To describe the interaction mechanisms between DCF and EHAC when reaching equilibrium at constant temperature, the experimental equilibrium data were fitted with adsorption isotherm models such as Freundlich, Langmuir, Dubinin-Radushkevich, and Temkin. The formulations of these models utilized in this study are given in Table S1. Langmuir isotherm presumes monolayer adsorption on uniform surface with no interactions between adsorbates [59]. The Langmuir isotherm parameters of DCF adsorption on EHAC were determined from the slope and intercept of the graph illustrated in Fig. 5(a) plotted C_e versus C_e/q_e , and its parameters at 25 °C are presented in Table 1. The maximum monolayer adsorption capacity for DCF adsorption on EHAC was calculated 147.06 mg/g, and the value of R^2 was computed 0.999 displaying good fitting of Langmuir isotherm to the experimental data of DCF adsorption on EHAC. Also, Langmuir constant (K_L) related to rate of adsorption was determined to be 0.589 L/mg, and the separation factor [60], the dimensionless equilibrium parameter (R_L) was determined to be between 0 and 1, suggesting favorable DCF adsorption on EHAC. The maximum adsorption capacities for DCF adsorption by various adsorbents are given in Table 2, in which it seems that the maximum DCF adsorption value of EHAC is not low compared to the others.

Freundlich isotherm presumes multilayer adsorption over heterogeneous surface with varied heat distribution

[69], and Freundlich isotherm parameters of DCF adsorption on EHAC, given in Table 1, were computed from the slope and intercept of the graph presented in Fig. 5(b) plotted $\ln C_e$ versus $\ln q_e$. Freundlich intensity constant (n) was calculated 2.309, which is lower than 10, meaning that DCF adsorption on EHAC is favorable [70]. Furthermore, Dubinin-Radushkevich isotherm model utilizes Gaussian energy distribution over heterogeneous surface [71], and Dubinin-Radushkevich isotherm parameters of DCF adsorption on EHAC, given in Table 1, were calculated from the slope and intercept of the graph given in Fig. 5(c) plotted ε^2 versus $\ln q_e$. If the mean energy of sorption (E) is lower than 8 kJ/mol, adsorption type is explained by physisorption process [72]. As seen in Table 1, the mean energy of sorption for DCF adsorption on EHAC at 25 °C was calculated 1.758 kJ/mol, which is lower than 8 kJ/mol, meaning that DCF adsorption by EHAC is managed by physisorption process with weak physical attraction forces, such as van der Waals forces and hydrogen-bonding. Moreover, Temkin isotherm considers that the adsorption heat of all molecules in the layer diminishes linearly with coverage owing to the interactions between adsorbate and adsorbent [73], and Temkin isotherm parameters of DCF adsorption on EHAC, given in Table 1, were calculated from the intercept and slope of the graph given in Fig. 5(d) plotted $\ln C_e$ versus q_e . The correlation coefficients of adsorption isotherms appear to be in the following order of Langmuir > Temkin > Freundlich > Dubinin-Radushkevich, which displays Langmuir

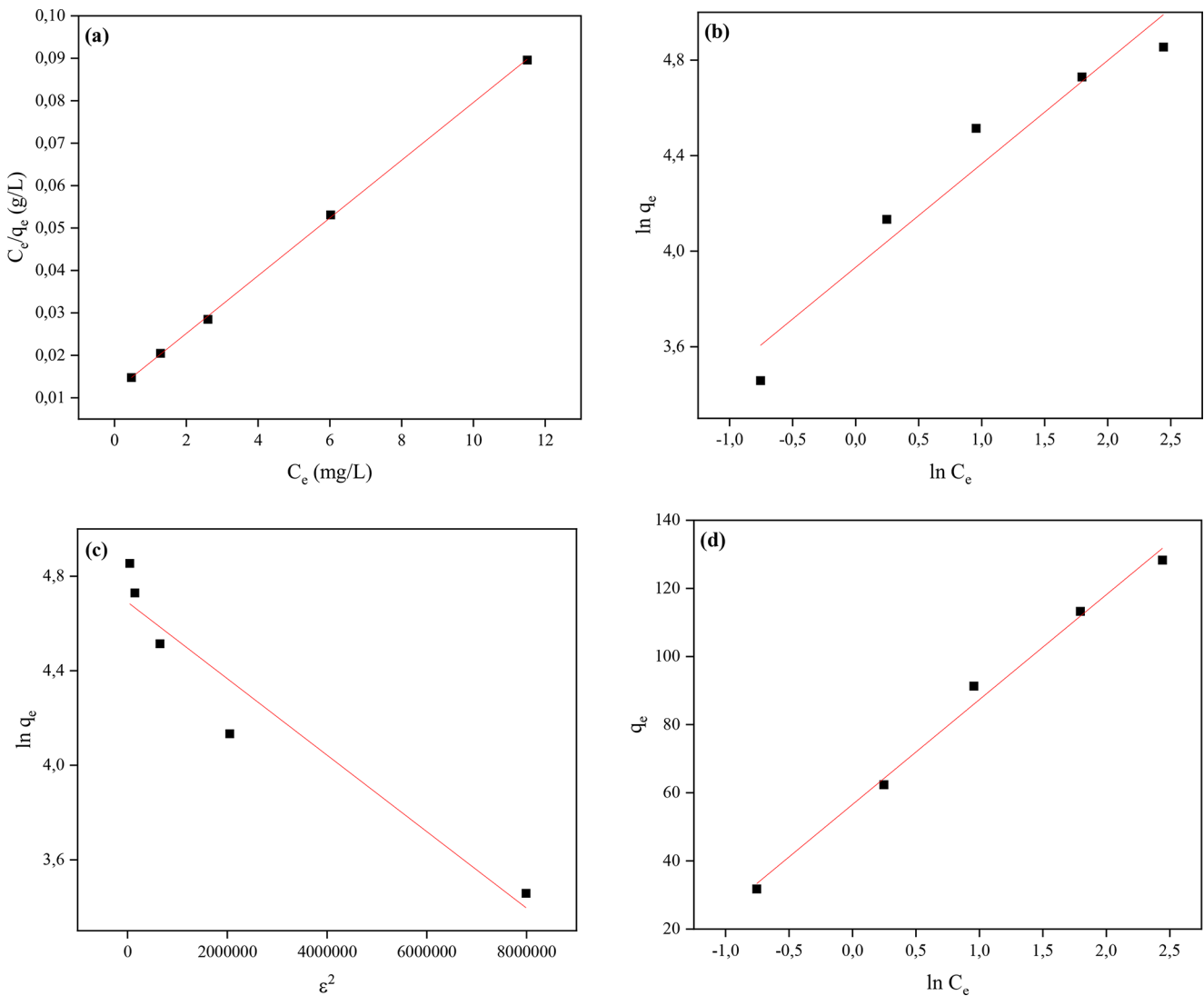


Fig. 5 (a) Langmuir, (b) Freundlich, (c) Dubinin-Radushkevich, and (d) Temkin isotherm plots of DCF adsorption by EHAC under conditions: where EHAC dosage=15 mg/50mL, DCF solution vol-

ume=50 mL, temperature=25 °C, contact time=180 min, agitation speed=160 rpm, and pH value=original

Table 1 Parameters of isotherm models for DCF adsorption on EHAC at 25 °C

Langmuir				Freundlich		
q_{max} (mg/g)	K_L (L/mg)	R^2	R_L	$1/n$	K_F (mg/g)(L/mg) ^{1/n}	R^2
147.06	0.589	0.999	$0 < R_L < 1$	0.433	51.032	0.918
Dubinin-Radushkevich (D-R)				Temkin		
q_d (mg/g)	β (mol ² /kJ ²)	E (kJ/mol)	R^2	A_T (L/g)	B_T (J/mol)	R^2
108.884	1.619×10^{-7}	1.758	0.902	6.280	80.507	0.989

isotherm is greatest fitted with the experimental data of DCF adsorption on EHAC.

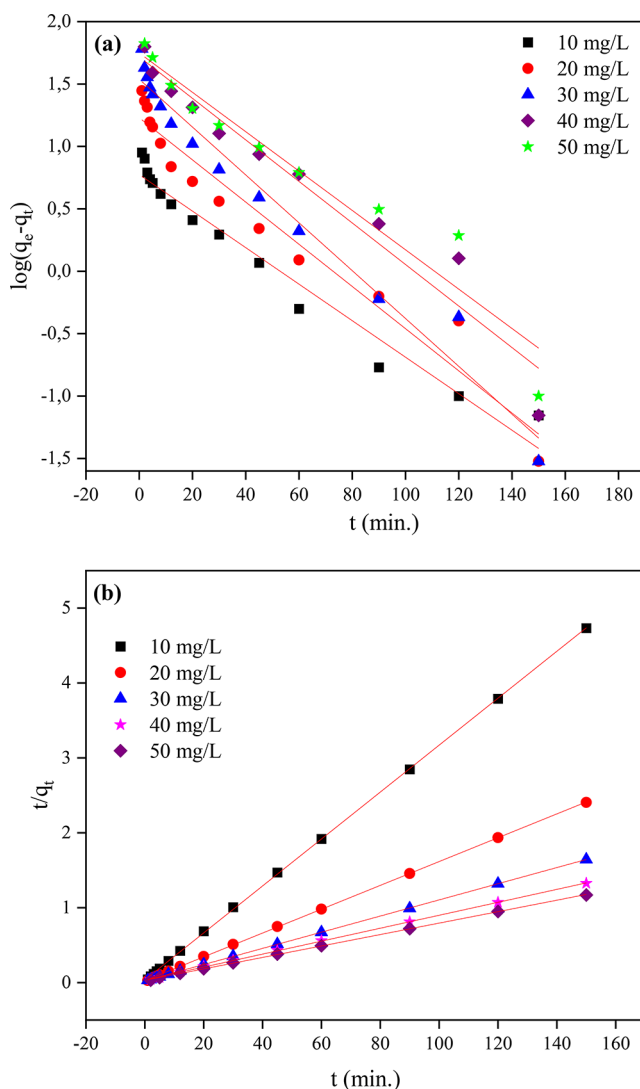
3.6 Adsorption kinetics

Pseudo-second order [74] and pseudo-first order [75] kinetic models whose formulations given in Table S2 were

applied to the kinetic experimental data of DCF adsorption on EHAC. While pseudo-first order model presumes that physisorption restricts particle adsorption rate on adsorbent, pseudo-second order model presumes that chemisorption is rate-restricting process [76]. Figure 6 displays the plots of pseudo-second order and pseudo-first order kinetics for DCF adsorption by EHAC, and their kinetic parameters

Table 2 Maximum adsorption capacities of DCF using various adsorbents

Adsorbent	q_m (mg/g)	References
Activated carbon (commercial)	83.00	[61]
AC from olive-waste cakes	56.20	[62]
AC from cocoa shell	63.47	[63]
Alginate/carbon films	29.90	[64]
AC form Sycamore balls	178.89	[65]
Expanded graphite	330.00	[66]
AC from Sugar cane bagasse	315.00	[58]
Nanoporous carbons from Argan nutshells	214.00	[67]
Graphene oxide nanosheets	128.74	[68]
AC from Einkorn husk	147.06	This work

**Fig. 6** (a) Pseudo-first-order kinetics and (b) pseudo-second-order kinetics for DCF adsorption by EHAC under conditions: where EHAC dosage = 15 mg/50 mL, DCF solution volume = 50 mL, temperature = 25 °C, agitation speed = 160 rpm, and pH value = original

are shown in Table 3. The experimental values ($q_{e, exp}$) for the pseudo-first order model are quite different from the calculated values (q_e), which indicates that the adsorption kinetics for DCF adsorption by EHAC do not follow the pseudo-first-order model. Also, R^2 values (0.961–0.927) determined for pseudo-first order model are lower than R^2 values (0.999) determined for pseudo-second order model. The experimental values ($q_{e, exp}$) for the pseudo-second order model are quite like the calculated values (q_e), proving the adsorption kinetics for DCF adsorption by EHAC follow the pseudo-second order model. This suggests that DCF adsorption process rate onto EHAC is restricted by chemisorption.

3.7 Adsorption mechanism

Fourier transform infrared spectrometer was operated to detect the FTIR peaks of EHAC and DCF+EHAC. These peaks are given in Fig. 7. The peaks between 3330 and 2887 cm^{-1} represent –OH and –COOH groups [77]. This peak becomes more prominent in the EHAC+DCF spectrum, proving that it arises from the COOH groups of DCF molecules adsorbed on EHAC. The peaks at 2395 and 2347 cm^{-1} were assigned to amino groups [78]. Therefore, the peaks between 2395 and 2316 cm^{-1} are another proof for DCF adsorption on EHAC, as seen in FTIR spectrum of EHAC+DCF compared to FTIR spectrum of EHAC. The broad peak at around 2100 cm^{-1} may correspond to allene (C=C=C) group [79]. The peak around 1574 cm^{-1} is ascribed to C=O functional group, while C–O functional group is seen at 1046 and 1092 cm^{-1} [80]. On the other hand, the band at 1580 cm^{-1} is ascribed to C=C stretching vibration in quinones and aromatic rings [81]. Moreover, the peak at 1500 cm^{-1} may be assigned to aromatic skeletal vibrations in EHAC. The peaks at 1444 and 1432 cm^{-1} might be assigned to O–H bending bands [79]. The broad band at ~1152 cm^{-1} corresponds C–O bonds in esters, acids, phenols, and ethers [79]. There are various bands in the region 900–700 cm^{-1} , which denotes out of plane C–H bending in aromatic structure [81, 82]. By considering the FTIR results, the solution pH, the pKa value of DCF, and the point of zero charge of EHAC, reasonable mechanisms for DCF adsorption on EHAC are illustrated at various pH values in Fig. 8. Detailed explanations about EHAC surface charge and the charge of DCF at different pH values were given in the section of 3.4. Effect of adsorption pH. As shown in Fig. 8, it is possible to occur various interactions between DCF molecules/ions and EHAC particles at various pH values, such as H-bonding, electrostatic attraction, electrostatic repulsion, π - π stacking.

Table 3 Parameters of kinetic models for DCF adsorption on EHAC at 25 °C

C_o (mg/L)	$q_{e, \text{exp}}$ (mg/g)	Pseudo-first order			Pseudo-second order		
		q_e (mg/g)	k_1 (1/min)	R^2	q_e (mg/g)	k_2 (g/mg min)	R^2
10	31.77	5.95	0.034	0.961	31.91	0.027	0.999
20	62.40	16.99	0.039	0.947	62.85	0.010	0.999
30	91.33	34.54	0.044	0.967	92.68	0.005	0.999
40	113.27	52.24	0.038	0.942	115.74	0.002	0.999
50	128.33	56.07	0.036	0.927	130.72	0.002	0.999

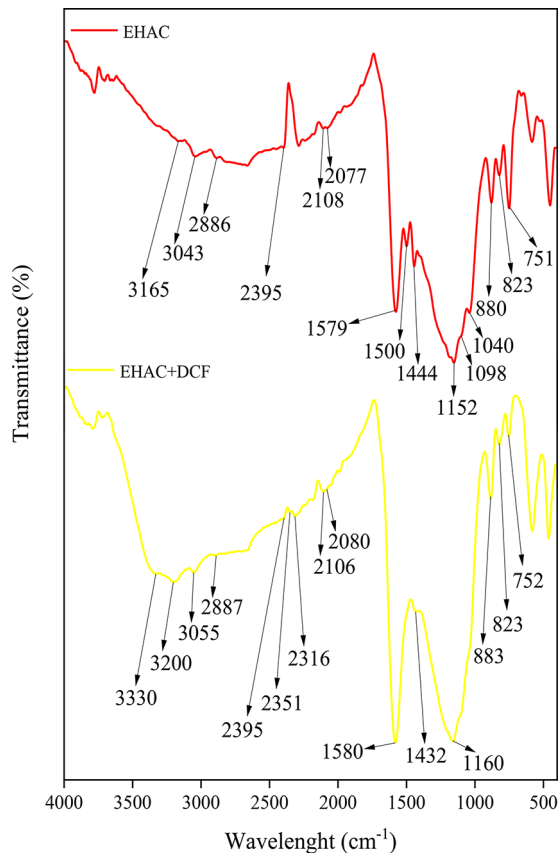


Fig. 7 FTIR spectra of EHAC and EHAC + DCF

The kinetic mechanism of DCF adsorption on EHAC was also studied by utilizing the intraparticle diffusion model [83] expressed by its formula below.

$$q_t = K_{pi}t^{1/2} + C_i \tag{4}$$

where q_t (mg/g) is the amount of adsorption at time t , K_{pi} (mg/g min^{1/2}) symbolizes intraparticle diffusion model rate constant, C_i refers the intercept, and t denotes adsorption time (min).

Figure S1 (a-e) illustrates the intraparticle diffusion model plots for DCF adsorption on EHAC at 25 °C when using DFC initial concentration of 10 – 50 mg/L. In the plots of intraparticle diffusion model, three regions are observed. The sharp region in first 5 min is rapid DCF adsorption by EHAC, which is caused by the boundary layer diffusion of

DCF molecules/ions from the bulk solution or the instantaneous DCF adsorption on EHAC exterior surface because of strong electrostatic attraction between EHAC and DCF. The second region is attributed to the intraparticle diffusion of DCF molecules/ions through EHAC pores, which is called the rate-restricting stage [84]. In this rate-restricting step, DCF molecules/ions are diffused into the internal parts of EHAC particles after EHAC exterior surfaces are quickly saturated with DCF molecules/ions in the first region, which provides slower process in second region than first region. The third phase is the final equilibrium stage, in which DCF adsorption process by EHAC begins to reduce because of the high affinity of DCF adsorbed on EHAC surface [85]. As shown in Figure S1 (a-e), the linear lines do not pass through the origin, which proves that intraparticle diffusion is not the merely rate controlling-step in DCF adsorption process by EHAC [76]. Moreover, the intraparticle diffusion model constants computed from the plots are shown in Table 4. The K_{pi} and C_i values for almost all initial concentrations at all three regions were determined to increase with increase in initial DCF concentration. The increasing initial DCF concentration in solution leads to higher driving force, thus higher DCF diffusion rate. Higher C_i value indicates higher boundary layer effect [85, 86]. The C_i values in Table 4 show that boundary layer effect becomes greater from first stage toward third stage for all initial concentrations.

3.8 Adsorption thermodynamics

The data obtained from temperature studies were applied to following Gibbs–Helmholtz and Van ‘t Hoff equations [57] to compute thermodynamic parameters, such as changes in entropy (ΔS , J/mol/K), enthalpy (ΔH , kJ/mol), and Gibbs free energy (ΔG , kJ/mol), and these calculated parameters were interpreted to describe thermodynamic behavior of DCF adsorption on EHAC.

$$\Delta G^0 = -RT \ln K \tag{5}$$

$$\ln K = \frac{\Delta S^0}{R} - \frac{\Delta H^0}{RT} \tag{6}$$

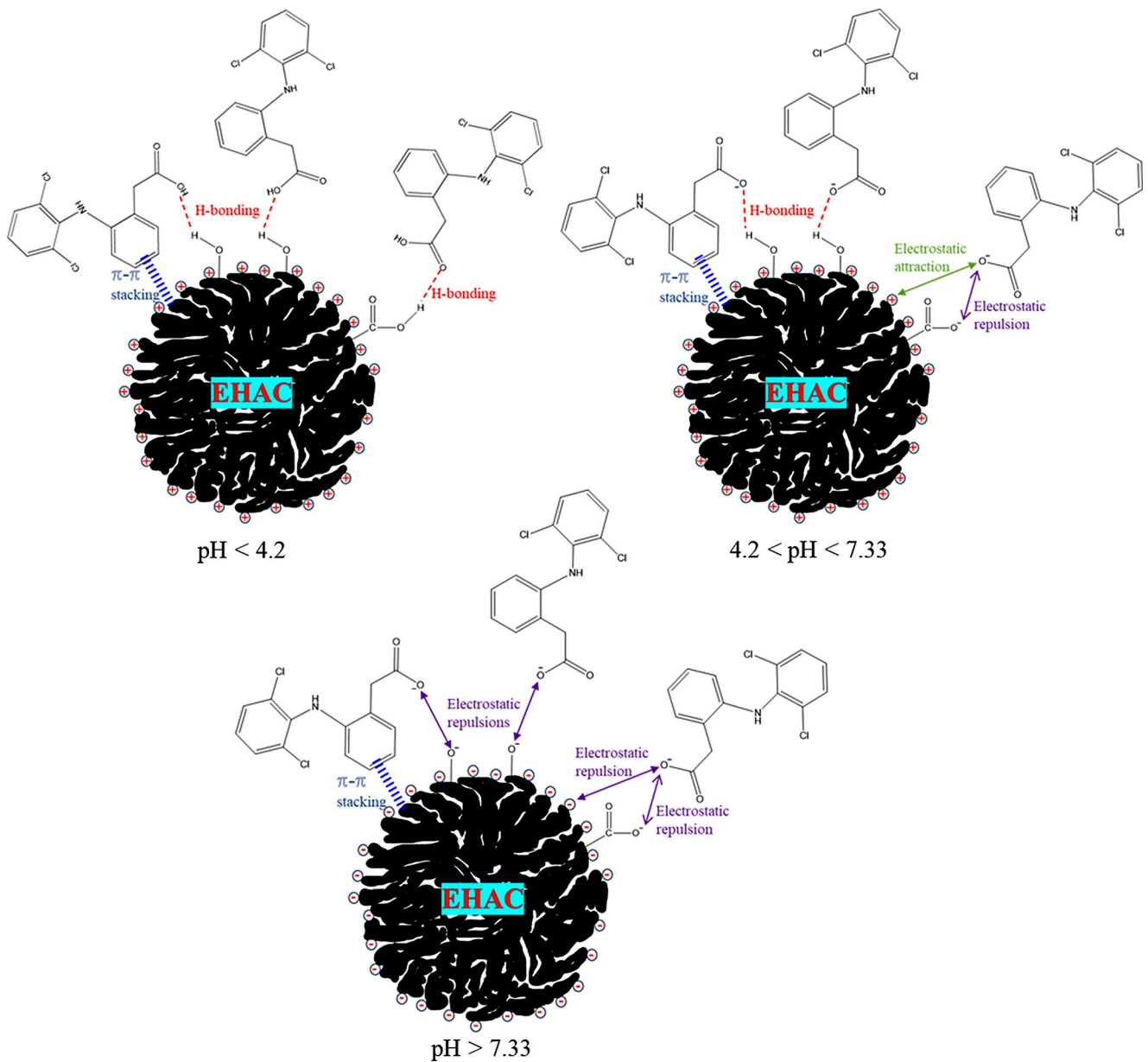


Fig. 8 Reasonable mechanisms for DCF adsorption on EHAC at various pH values

where $K [(C_0 - C_e)/C_e]$ symbolizes equilibrium constant [87]. T (K) and R represent the absolute temperature and the universal gas constant (8.314 kJ/mol), respectively. The thermodynamic parameter values calculated are presented with their conditions in Table 5. The thermodynamic parameter values were calculated by considering each initial concentration used in this study, separately, because the actual thermodynamic parameters depend on adsorption temperature and pH also as well as the relative concentration of adsorbate and adsorbent in solution, changing the equilibrium points. To reveal the initial DCF concentration effect on thermodynamic parameters, EHAC concentrations in solutions were kept constant (15 mg/50mL)

for thermodynamic study experiments. Negative enthalpy values between -24.645 and -4.265 kJ/mol indicate that DCF adsorption on EHAC is exothermic. When increasing adsorption temperature, the negative ΔG values showing DCF adsorption onto EHAC to be spontaneous and feasible increase for all initial DCF concentrations. The noteworthy point here is that the increase in ΔG values is getting higher for each adsorption temperature while initial DCF concentration in solution is increasing from 10 mg/L to 50 mg/L. This is because the increase of DCF ions/molecules in solution may interact more with each other's, which might reduce the adsorption affinities between DCF and EHAC. Also, negative ΔS values between -0.058 and -0.004 kJ/

Table 4 Intraparticle diffusion model constants for DCF adsorption onto EHAC at 25 °C

	DFC initial concentration (mg/L)				
	10	20	30	40	50
K_{p1} (mg/g min ^{1/2})	15.231	25.047	32.776	33.469	35.305
K_{p2} (mg/g min ^{1/2})	0.9011	2.830	5.413	6.003	5.504
K_{p3} (mg/g min ^{1/2})	0.0804	0.220	0.350	1.044	0.864
C_1	2.2543	2.912	1.903	0.789	3.156
C_2	24.857	43.046	54.200	65.659	81.279
C_3	30.736	59.568	86.932	100.080	117.078
$(R_1)^2$	0.857	0.906	0.991	0.995	0.931
$(R_2)^2$	0.960	0.864	0.918	0.953	0.922
$(R_3)^2$	0.796	0.935	0.769	0.858	0.898

Table 5 Thermodynamic parameters for DCF adsorption onto EHAC under conditions: where EHAC dosage = 15 mg/50mL, DCF solution volume = 50 mL, agitation speed = 160 rpm, contact time = 180 min, and pH value = original

Initial DCF Concentration (mg/L)	Temperature (°C)	ΔG (kJ/mol)	ΔH (kJ/mol)	ΔS (kJ/mol/K)
10	25	-7.460	-24.645	-0.058
	35	-6.328		
	45	-6.320		
20	25	-6.650	-21.173	-0.049
	35	-5.881		
	45	-5.682		
30	25	-5.838	-14.571	-0.029
	35	-5.472		
	45	-5.254		
40	25	-4.290	-7.950	-0.012
	35	-4.062		
	45	-4.047		
50	25	-2.995	-4.265	-0.004
	35	-2.883		
	45	-2.912		

mol/K, denoting a decline in randomness at the solution/solid interface and no important alteration consisting in inner structure of adsorbent by sorption [88].

4 Conclusions

This study investigates the DCF adsorption in aqueous solution by utilizing EHAC under various conditions in a batch mode. It was determined that the solution pH greatly affected the DCF adsorption on EHAC. Equilibrium data were greatest fitted by Langmuir isotherm model compared to Temkin, Freundlich, and Dubinin-Radushkevich isotherm models. The maximum monolayer adsorption capacity for DCF adsorption on EHAC at 25 °C was computed

147.06 mg/g. Adsorption kinetic data displayed that DCF adsorption on EHAC obeys the pseudo-second order model. Also, DCF adsorption mechanisms were proposed at various pH values by using FTIR and pH data obtained from DCF adsorption on EHAC. Moreover, intraparticle diffusion was not merely rate controlling step in DCF adsorption process by EHAC, and mostly higher DCF diffusion rate was observed when increasing initial DCF concentration in solution. In the thermodynamic studies, the negative ΔG values increase when increasing adsorption temperature for all initial DCF concentrations, and DCF adsorption process by EHAC was exothermic, spontaneous, and feasible.

Supplementary Information The online version contains supplementary material available at <https://doi.org/10.1007/s10450-024-00479-2>.

Author contributions BK: Conceptualization, Methodology, Validation, Formal analysis, Investigation, Visualization, Writing - Review & Editing. OÜ: Conceptualization, Methodology, Formal analysis, Investigation, Visualization, Writing - Original Draft, Writing - Review & Editing. ÜG: Conceptualization, Methodology, Validation, Investigation, Resources, Writing - Review & Editing.

Funding No funding was received to assist with the preparation of this manuscript. Open access funding provided by the Scientific and Technological Research Council of Türkiye (TÜBİTAK).

Data availability No datasets were generated or analysed during the current study.

Declarations

Ethical approval This is not applicable in this article.

Conflict of interest The authors declare no competing interest.

Open Access This article is licensed under a Creative Commons Attribution 4.0 International License, which permits use, sharing, adaptation, distribution and reproduction in any medium or format, as long as you give appropriate credit to the original author(s) and the source, provide a link to the Creative Commons licence, and indicate if changes were made. The images or other third party material in this article are included in the article’s Creative Commons licence, unless indicated otherwise in a credit line to the material. If material is not included in the article’s Creative Commons licence and your intended use is not permitted by statutory regulation or exceeds the permitted use, you will need to obtain permission directly from the copyright holder. To view a copy of this licence, visit <http://creativecommons.org/licenses/by/4.0/>.

References

1. Huber, C., Preis, M., Harvey, P.J., Grosse, S., Letzel, T., Schröder, P.: Emerging pollutants and plants—metabolic activation of diclofenac by peroxidases. *Chemosphere*. **146**, 435–441 (2016). <https://doi.org/10.1016/j.chemosphere.2015.12.059>

2. Lu, Y., Fan, L., Yang, L.Y., Huang, F., Ouyang, X.K.: PEI-modified core-shell/bead-like amino silica enhanced poly (vinyl alcohol)/chitosan for diclofenac sodium efficient adsorption. *Carbohydr. Polym.* **229**, 115459 (2020). <https://doi.org/10.1016/j.carbpol.2019.115459>
3. Malefane, M.E., Feleni, U., Kuvarega, A.T.: Cobalt (II/III) oxide and tungsten (VI) oxide pn heterojunction photocatalyst for photodegradation of diclofenac sodium under visible light. *J. Environ. Chem. Eng.* **8**(2), 103560 (2020). <https://doi.org/10.1016/j.jece.2019.103560>
4. Machado, T.S., Crestani, L., Marchezi, G., Melara, F., de Mello, J.R., Dotto, G.L., Piccin, J.S.: Synthesis of glutaraldehyde-modified silica/chitosan composites for the removal of water-soluble diclofenac sodium. *Carbohydr. Polym.* **277**, 118868 (2022). <https://doi.org/10.1016/j.carbpol.2021.118868>
5. Huynh, N.C., Nguyen, T.T.T., Nguyen, D.T.C., Van Tran, T.: Occurrence, toxicity, impact and removal of selected non-steroidal anti-inflammatory drugs (NSAIDs): A review. *Sci. Total Environ.* **898**, 165317 (2023). <https://doi.org/10.1016/j.scitotenv.2023.165317>
6. Guo, W., Chen, Y., Cui, L., Xu, N., Wang, M., Sun, Y., Yan, Y.: Nano-hydroxyapatite/carbon nanotube: An excellent anode modifying material for improving the power output and diclofenac sodium removal of microbial fuel cells. *Bioelectrochemistry.* **154**, 108523 (2023). <https://doi.org/10.1016/j.bioelechem.2023.108523>
7. Todd, P.A., Sorkin, E.M.: Diclofenac sodium: A reappraisal of its pharmacodynamic and pharmacokinetic properties, and therapeutic efficacy. *Drugs.* **35**, 244–285 (1988). <https://doi.org/10.2165/00003495-198835030-00004>
8. Palomo, M.E., Ballesteros, M.P., Frutos, P.: Analysis of diclofenac sodium and derivatives. *J. Pharm. Biomed. Anal.* **21**(1), 83–94 (1999). [https://doi.org/10.1016/S0731-7085\(99\)00089-8](https://doi.org/10.1016/S0731-7085(99)00089-8)
9. Fini, A., Garuti, M., Fazio, G., Alvarez-Fuentes, J., Holgado, M.A.: Diclofenac salts. I. Fractal and thermal analysis of sodium and potassium diclofenac salts. *J. Pharm. Sci.* **90**(12), 2049–2057 (2001). <https://doi.org/10.1002/jps.1156>
10. Suhail, M., Khan, A., Rosenholm, J.M., Minhas, M.U., Wu, P.C.: Fabrication and characterization of diclofenac sodium loaded hydrogels of sodium alginate as sustained release carrier. *Gels.* **7**(1), 10 (2021). <https://doi.org/10.3390/gels7010010>
11. Atzeni, F., Masala, I.F., Sarzi-Puttini, P.: A review of chronic musculoskeletal pain: Central and peripheral effects of diclofenac. *Pain Ther.* **7**, 163–177 (2018). <https://doi.org/10.1007/s40122-018-0100-2>
12. Zhang, Y., Geißen, S.U., Gal, C.: Carbamazepine and diclofenac: Removal in wastewater treatment plants and occurrence in water bodies. *Chemosphere.* **73**(8), 1151–1161 (2008). <https://doi.org/10.1016/j.chemosphere.2008.07.086>
13. Luongo, G., Guida, M., Siciliano, A., Libralato, G., Saviano, L., Amoresano, A., Previtera, L., Di Fabio, G., Zarrelli, A.: Oxidation of diclofenac in water by sodium hypochlorite: Identification of new degradation by-products and their ecotoxicological evaluation. *J. Pharm. Biomed. Anal.* **194**, 113762 (2021). <https://doi.org/10.1016/j.jpba.2020.113762>
14. Latif, S., Liaqat, A., Imran, M., Javaid, A., Hussain, N., Jesionowski, T., Bilal, M.: Development of zinc ferrite nanoparticles with enhanced photocatalytic performance for remediation of environmentally toxic pharmaceutical waste diclofenac sodium from wastewater. *Environ. Res.* **216**, 114500 (2023). <https://doi.org/10.1016/j.envres.2022.114500>
15. Alessandretti, I., Rigueto, C.V.T., Nazari, M.T., Rosseto, M., Dettmer, A.: Removal of diclofenac from wastewater: A comprehensive review of detection, characteristics and tertiary treatment techniques. *J. Environ. Chem. Eng.* **9**(6), 106743 (2021). <https://doi.org/10.1016/j.jece.2021.106743>
16. Lonappan, L., Brar, S.K., Das, R.K., Verma, M., Surampalli, R.Y.: Diclofenac and its transformation products: Environmental occurrence and toxicity—a review. *Environ. Int.* **96**, 127–138 (2016). <https://doi.org/10.1016/j.envint.2016.09.014>
17. Letzel, M., Metzner, G., Letzel, T.: Exposure assessment of the pharmaceutical diclofenac based on long-term measurements of the aquatic input. *Environ. Int.* **35**(2), 363–368 (2009). <https://doi.org/10.1016/j.envint.2008.09.002>
18. Lee, J., Ji, K., Kho, Y.L., Kim, P., Choi, K.: Chronic exposure to diclofenac on two freshwater cladocerans and Japanese medaka. *Ecotoxicol. Environ. Saf.* **74**(5), 1216–1225 (2011). <https://doi.org/10.1016/j.ecoenv.2011.03.014>
19. Guiloski, I.C., Ribas, J.L.C., da Silva Pereira, L., Neves, A.P.P., de Assis, H.C.S.: Effects of trophic exposure to dexamethasone and diclofenac in freshwater fish. *Ecotoxicol. Environ. Saf.* **114**, 204–211 (2015). <https://doi.org/10.1016/j.ecoenv.2014.11.020>
20. Hiba, Z.I.N.D., Mondamert, L., Remaury, Q.B., Cleon, A., Leitner, N.K.V., Labanowski, J.: Occurrence of carbamazepine, diclofenac, and their related metabolites and transformation products in a French aquatic environment and preliminary risk assessment. *Water Res.* **196**, 117052 (2021)
21. Mirzaee, S.A., Noorimotlagh, Z., Ahmadi, M., Rahim, F., Martinez, S.S., Nourmohammadi, A., Jaafarzadeh, N.: The possible oxidative stress and DNA damage induced in Diclofenac-exposed non-target organisms in the aquatic environment: A systematic review. *Ecol. Indic.* **131**, 108172 (2021). <https://doi.org/10.1016/j.ecolind.2021.108172>
22. Duarte, J.A.P., Ribeiro, A.K.N., de Carvalho, P., Bortolini, J.C., Ostroski, I.C.: Emerging contaminants in the aquatic environment: Phytoplankton structure in the presence of sulfamethoxazole and diclofenac. *Environ. Sci. Pollut Res.* **30**(16), 46604–46617 (2023). <https://doi.org/10.1007/s11356-023-25589-2>
23. Bonnefille, B., Gomez, E., Courant, F., Escande, A., Fenet, H.: Diclofenac in the marine environment: A review of its occurrence and effects. *Mar. Pollut Bull.* **131**, 496–506 (2018). <https://doi.org/10.1016/j.marpolbul.2018.04.053>
24. Sathishkumar, P., Meena, R.A.A., Palanisami, T., Ashokkumar, V., Palvannan, T., Gu, F.L.: Occurrence, interactive effects and ecological risk of diclofenac in environmental compartments and biota—a review. *Sci. Total Environ.* **698**, 134057 (2020). <https://doi.org/10.1016/j.scitotenv.2019.134057>
25. Corada-Fernández, C., Jiménez-Martínez, J., Candela, L., González-Mazo, E., Lara-Martín, P.A.: Occurrence and spatial distribution of emerging contaminants in the unsaturated zone. Case study: Guadalete River basin (Cadiz, Spain). *Chemosphere* **119**, S131–S137 (2015). <https://doi.org/10.1016/j.chemosphere.2014.04.098>
26. Ashfaq, M., Khan, K.N., Rehman, M.S.U., Mustafa, G., Nazar, M.F., Sun, Q., Iqbal, J., Mulla, S.I., Yu, C.P.: Ecological risk assessment of pharmaceuticals in the receiving environment of pharmaceutical wastewater in Pakistan. *Ecotoxicol. Environ. Saf.* **136**, 31–39 (2017). <https://doi.org/10.1016/j.ecoenv.2016.10.029>
27. Mondal, S., Wickramasinghe, S.R.: Produced water treatment by nanofiltration and reverse osmosis membranes. *J. Membr. Sci.* **322**(1), 162–170 (2008). <https://doi.org/10.1016/j.memsci.2008.05.039>
28. Üner, O., Körükçü, B.C., Özcan, C.: Adsorption application of activated carbon from ripe black Locust seed pods for wastewater taken from Ergene River. *Turk. Int. J. Environ. Anal. Chem.* **103**(9), 2152–2167 (2023). <https://doi.org/10.1080/03067319.2021.1889533>
29. Peng, H., Guo, J.: Removal of chromium from wastewater by membrane filtration, chemical precipitation, ion exchange, adsorption electrocoagulation, electrochemical reduction, electro-dialysis, electrodeionization, photocatalysis and nanotechnology:

- A review. *Environ. Chem. Lett.* **18**, 2055–2068 (2020). <https://doi.org/10.1007/s10311-020-01058-x>
30. Zhang, Y., Duan, X.: Chemical precipitation of heavy metals from wastewater by using the synthetical magnesium hydroxy carbonate. *Water Sci. Technol.* **81**(6), 1130–1136 (2020). <https://doi.org/10.2166/wst.2020.208>
 31. Jabbar, K.Q., Barzinjy, A.A., Hamad, S.M.: Iron oxide nanoparticles: Preparation methods, functions, adsorption and coagulation/flocculation in wastewater treatment. *Environ. Nanotechnol. Monit. Manag.* **17**, 100661 (2022). <https://doi.org/10.1016/j.enmm.2022.100661>
 32. Shahedi, A., Darban, A.K., Taghipour, F., Jamshidi-Zanjani, A.: A review on industrial wastewater treatment via electrocoagulation processes. *Curr. Opin. Electrochem.* **22**, 154–169 (2020). <https://doi.org/10.1016/j.coelec.2020.05.009>
 33. Yang, Y., Wang, L., Xiang, F., Zhao, L., Qiao, Z.: Activated sludge microbial community and treatment performance of wastewater treatment plants in industrial and municipal zones. *Int. J. Environ. Res. Public Health.* **17**(2), 436 (2020). <https://doi.org/10.3390/ijerph17020436>
 34. Foresti, E., Zaiat, M., Vallero, M.: Anaerobic processes as the core technology for sustainable domestic wastewater treatment: Consolidated applications, new trends, perspectives, and challenges. *Rev. Environ. Sci. Biotechnol.* **5**, 3–19 (2006). <https://doi.org/10.1007/s11157-005-4630-9>
 35. Chakraborty, R., Asthana, A., Singh, A.K., Jain, B., Susan, A.B.H.: Adsorption of heavy metal ions by various low-cost adsorbents: A review. *Int. J. Environ. Anal. Chem.* **102**(2), 342–379 (2022). <https://doi.org/10.1080/03067319.2020.1722811>
 36. Oba, S.N., Ighalo, J.O., Aniagor, C.O., Igwegbe, C.A.: Removal of ibuprofen from aqueous media by adsorption: A comprehensive review. *Sci. Total Environ.* **780**, 146608 (2021). <https://doi.org/10.1016/j.scitotenv.2021.146608>
 37. Zhang, Y., Zhao, M., Cheng, Q., Wang, C., Li, H., Han, X., Fan, Z., Su, G., Pan, D., Li, Z.: Research progress of adsorption and removal of heavy metals by chitosan and its derivatives: A review. *Chemosphere.* **279**, 130927 (2021). <https://doi.org/10.1016/j.chemosphere.2021.130927>
 38. He, J., Hong, S., Zhang, L., Gan, F., Ho, Y.S.: Equilibrium and thermodynamic parameters of adsorption of methylene blue onto rectorite. *Fresenius Environ. Bull.* **19**(11), 2651–2656 (2010)
 39. Rashid, R., Shafiq, I., Akhter, P., Iqbal, M.J., Hussain, M.: A state-of-the-art review on wastewater treatment techniques: The effectiveness of adsorption method. *Environ. Sci. Pollut Res.* **28**, 9050–9066 (2021). <https://doi.org/10.1007/s11356-021-12395-x>
 40. Majd, M.M., Kordzadeh-Kermani, V., Ghalandari, V., Askari, A., Sillanpää, M.: Adsorption isotherm models: A comprehensive and systematic review (2010–2020). *Sci. Total Environ.* **812**, 151334 (2022). <https://doi.org/10.1016/j.scitotenv.2021.151334>
 41. Lu, Y.C., Kooh, M.R.R., Lim, L.B.L., Priyantha, N.: Effective and simple NaOH-modification method to remove methyl violet dye via *Ipomoea aquatica* roots. *Adsorpt. Sci. Technol.* 1–12 (2021). (2021). <https://doi.org/10.1155/2021/5932222>
 42. Suhaimi, N., Kooh, M.R.R., Lim, C.M., Chao, C.T.C., Chau, Y.F.C., Mahadi, A.H., Chiang, H.P., Hassan, N.H.H., Thotagamuge, R.: The use of gigantochloa bamboo-derived biochar for the removal of methylene blue from aqueous solution. *Adsorpt. Sci. Technol.* 1–12 (2022). (2022). <https://doi.org/10.1155/2022/8245797>
 43. Han, Q., Wang, J., Goodman, B.A., Xie, J., Liu, Z.: High adsorption of methylene blue by activated carbon prepared from phosphoric acid treated eucalyptus residue. *Powder Technol.* **366**, 239–248 (2020). <https://doi.org/10.1016/j.powtec.2020.02.013>
 44. Sultana, M., Rownok, M.H., Sabrin, M., Rahaman, M.H., Alam, S.N.: A review on experimental chemically modified activated carbon to enhance dye and heavy metals adsorption. *Clean. Eng. Technol.* **6**, 100382 (2022). <https://doi.org/10.1016/j.clet.2021.100382>
 45. Tay, T., Ucar, S., Karagöz, S.: Preparation and characterization of activated carbon from waste biomass. *J. Hazard. Mater.* **165**(1–3) (2009). 481–485 <https://doi.org/10.1016/j.jhazmat.2008.10.011>
 46. Gurten, I.I., Ozmak, M., Yagmur, E., Aktas, Z.: Preparation and characterisation of activated carbon from waste tea using K₂CO₃. *Biomass Bioenergy.* **37**, 73–81 (2012). <https://doi.org/10.1016/j.biombioe.2011.12.030>
 47. Guo, Y., Tan, C., Sun, J., Li, W., Zhang, J., Zhao, C.: Porous activated carbons derived from waste sugarcane bagasse for CO₂ adsorption. *Chem. Eng. J.* **381**, 122736 (2020). <https://doi.org/10.1016/j.cej.2019.122736>
 48. Gupta, S.A., Vishesh, Y., Sarvshrestha, N., Bhardwaj, A.S., Kumar, P.A., Topare, N.S., Raut-Jadhav, S., Bokil, S.A., Khan, A.: Adsorption isotherm studies of Methylene blue using activated carbon of waste fruit peel as an adsorbent. *Mater. Today: Proc.* **57**, 1500–1508 (2022). <https://doi.org/10.1016/j.matpr.2021.12.044>
 49. Vakili, A., Zinatizadeh, A.A., Rahimi, Z., Zinadini, S., Mohammedi, P., Azizi, S., Karami, A., Abdulgader, M.: The impact of activation temperature and time on the characteristics and performance of agricultural waste-based activated carbons for removing dye and residual COD from wastewater. *J. Clean. Prod.* **382**, 134899 (2023). <https://doi.org/10.1016/j.jclepro.2022.134899>
 50. FAO: Wheat Landraces in Farmers' Fields in Turkey: National Survey, Collection, and Conservation, 2009–2014, by Mustafa Kan, Murat Küçükçongar, Mesut Keser, Alexey Morgounov, Hafiz Muminjanov, Fatih Özdemir, Calvin Qualset. (2015)
 51. Nakov, G., Brandolini, A., Ivanova, N., Dimov, I., Stamatovska, V.: The effect of einkorn (*Triticum monococcum* L.) whole meal flour addition on physico-chemical characteristics, biological active compounds and in vitro starch digestion of cookies. *J. Cereal Sci.* **83**, 116–122 (2018). <https://doi.org/10.1016/j.jcs.2018.08.004>
 52. Brandolini, A., Lucisano, M., Mariotti, M., Hidalgo, A.: A study on the quality of einkorn (*Triticum monococcum* L. ssp. *Monococcum*) pasta. *J. Cereal Sci.* **82**, 57–64 (2018). <https://doi.org/10.1016/j.jcs.2018.05.010>
 53. Kocabiyik, B., Bayrak, Y.: Application of a Bio-waste Einkorn (*Triticum monococcum* L.) husks Adsorbent for removal of Metanil Yellow and Methylene Blue from Aqueous Media with Equilibrium, Kinetic, and Thermodynamic studies. *Water Air Soil. Pollut.* **235**(3), 200 (2024). <https://doi.org/10.1007/s11270-024-06996-8>
 54. Acemioğlu, B.: Batch kinetic study of sorption of methylene blue by perlite. *Chem. Eng. J.* **106**(1), 73–81 (2005). <https://doi.org/10.1016/j.cej.2004.10.005>
 55. Daoud, M., Benturki, O., Girods, P., Donnot, A., Fontana, S.: Adsorption ability of activated carbons from Phoenix dactylifera rachis and Ziziphus jujube stones for the removal of commercial dye and the treatment of dyestuff wastewater. *Microchem J.* **148**, 493–502 (2019). <https://doi.org/10.1016/j.microc.2019.05.022>
 56. Milonjić, S.K., Ruvarac, A.L., Šušić, M.V.: The heat of immersion of natural magnetite in aqueous solutions. *Thermochim. Acta.* **11**(3), 261–266 (1975). [https://doi.org/10.1016/0040-6031\(75\)85095-7](https://doi.org/10.1016/0040-6031(75)85095-7)
 57. Aljeboree, A.M., Alshirifi, A.N., Alkaim, A.F.: Kinetics and equilibrium study for the adsorption of textile dyes on coconut shell activated carbon. *Arab. J. Chem.* **10**, S3381–S3393 (2017). <https://doi.org/10.1016/j.arabjc.2014.01.020>
 58. El Naga, A.O.A., El Saied, M., Shaban, S.A., El Kady, F.Y.: Fast removal of diclofenac sodium from aqueous solution using sugar cane bagasse-derived activated carbon. *J. Mol. Liq.* **285**, 9–19 (2019). <https://doi.org/10.1016/j.molliq.2019.04.062>
 59. Langmuir, I.: The constitution and fundamental properties of solids and liquids. Part I. solids. *J. Am. Chem. Soc.* **38**(11), 2221–2295 (1916). <https://doi.org/10.1021/ja02268a002>

60. Weber, T.W., Chakkravorti, R.K.: Pore and solid diffusion models for fixedbed adsorbers. *AIChE J.* **20**, 228 (1974). <https://doi.org/10.1002/aic.690200204>
61. Bhadra, B.N., Seo, P.W., Jhung, S.H.: Adsorption of diclofenac sodium from water using oxidized activated carbon. *Chem. Eng. J.* **301**, 27–34 (2016). <https://doi.org/10.1016/j.cej.2016.04.143>
62. Baccar, R., Sarrà, M., Bouzid, J., Feki, M., Blánquez, P.: Removal of pharmaceutical compounds by activated carbon prepared from agricultural by-product. *Chem. Eng. J.* **211**, 310–317 (2012). <https://doi.org/10.1016/j.cej.2012.09.099>
63. Saucier, C., Adebayo, M.A., Lima, E.C., Cataluña, R., Thue, P.S., Prola, L.D., Puchana-Rosero, M.J., Machado, F.M., Pavan, F.A., Dotto, G.L.: Microwave-assisted activated carbon from cocoa shell as adsorbent for removal of sodium diclofenac and nimesulide from aqueous effluents. *J. Hazard. Mater.* **289**, 18–27 (2015). <https://doi.org/10.1016/j.jhazmat.2015.02.026>
64. Shamsudin, M.S., Azha, S.F., Sellaoui, L., Badawi, M., Bonilla-Petriciolet, A., Ismail, S.: Performance and interactions of diclofenac adsorption using Alginate/Carbon-based films: Experimental investigation and statistical physics modelling. *Chem. Eng. J.* **428**, 131929 (2022). <https://doi.org/10.1016/j.cej.2021.131929>
65. Avcu, T., Üner, O., Geçgel, Ü.: Adsorptive removal of diclofenac sodium from aqueous solution onto sycamore ball activated carbon—isothersms, kinetics, and thermodynamic study. *Surf. Interfaces.* **24**, 101097 (2021). <https://doi.org/10.1016/j.surfin.2021.101097>
66. Vedenyapina, M.D., Borisova, D.A., Simakova, A.P., Proshina, L.P., Vedenyapin, A.A.: Adsorption of diclofenac sodium from aqueous solutions on expanded graphite. *Solid Fuel Chem.* **47**, 59–63 (2013). <https://doi.org/10.3103/S0361521912060134>
67. Mokhati, A., Benturki, O., Bernardo, M., Kecira, Z., Matos, I., Lapa, N., Soares, O.S.G.P., Ventura, M., Botelho do Rego, A.M., Fonseca, I.M.: Nanoporous carbons prepared from argan nutshells as potential removal agents of diclofenac and paroxetine. *J. Mol. Liq.* **326**, 115368 (2021). <https://doi.org/10.1016/j.molliq.2021.115368>
68. Guerra, A.C.S., de Andrade, M.B., Tonial dos Santos, T.R., Bergamasco, R.: Adsorption of sodium diclofenac in aqueous medium using graphene oxide nanosheets. *Environ. Technol.* **42**(16), 2599–2609 (2021). <https://doi.org/10.1080/09593330.2019.1707882>
69. Freundlich, H.: Über die adsorption in lösungen. *Z. für Phys. Chem.* **57**(1), 385–470 (1907). <https://doi.org/10.1515/zpch-1907-5723>
70. Güzel, F., Koyuncu, F.: Adsorptive removal of diclofenac sodium from aqueous solution via industrial processed citrus solid waste-based activated carbon: Optimization, kinetics, equilibrium, thermodynamic, and reusability analyses. *Biomass Convers. Biorefin.* **13**(3), 2401–2412 (2023). <https://doi.org/10.1007/s13399-021-01969-x>
71. Foo, K.Y., Hameed, B.H.: Insights into the modeling of adsorption isotherm systems. *Chem. Eng. J.* **156**(1), 2–10 (2010). <https://doi.org/10.1016/j.cej.2009.09.013>
72. Ragadhita, R.I.S.T.I., Nandiyanto, A.B.D.: Curcumin adsorption on zinc imidazole framework-8 particles: Isotherm adsorption using Langmuir, Freundlich, Temkin, and Dubinin-Radushkevich models. *J. Eng. Sci. Technol.* **17**(2), 1078–1089 (2022)
73. Temkin, M.J., Pyzhev, V.: Recent modifications to Langmuir isotherms. *Acta Physicochim URSS.* **12**, 217–225 (1940)
74. Ho, Y.S., McKay, G.: Pseudo-second order model for sorption processes. *Process. Biochem.* **34**(5), 451–465 (1999). [https://doi.org/10.1016/S0032-9592\(98\)00112-5](https://doi.org/10.1016/S0032-9592(98)00112-5)
75. Lagergren, S.: Zur Theorie Der Sogenannten adsorption geloster stoffe. *Kungliga Svenska Vetenskapsakademiens Handlingar.* **24**, 1–39 (1898)
76. Sumalinog, D.A.G., Capareda, S.C., de Luna, M.D.G.: Evaluation of the effectiveness and mechanisms of acetaminophen and methylene blue dye adsorption on activated biochar derived from municipal solid wastes. *J. Environ. Manage.* **210**, 255–262 (2018). <https://doi.org/10.1016/j.jenvman.2018.01.010>
77. Shen, W., Li, Z., Liu, Y.: Surface chemical functional groups modification of porous carbon. *Recent. Pat. Chem. Eng.* **1**(1), 27–40 (2008)
78. Ching, S.L., Yusoff, M.S., Aziz, H.A., Umar, M.: Influence of impregnation ratio on coffee ground activated carbon as landfill leachate adsorbent for removal of total iron and orthophosphate. *Desalination.* **279**(1–3) (2011). 225–234 <https://doi.org/10.1016/j.desal.2011.06.011>
79. Islam, M.S., Ang, B.C., Gharekhani, S., Afifi, A.B.M.: Adsorption capability of activated carbon synthesized from coconut shell. *Carbon Lett.* **20**, 1–9 (2016). <https://doi.org/10.5714/CL.2016.20.001>
80. Ai, L., Zhang, C., Liao, F., Wang, Y., Li, M., Meng, L., Jiang, J.: Removal of methylene blue from aqueous solution with magnetite loaded multi-wall carbon nanotube: Kinetic, isotherm and mechanism analysis. *J. Hazard. Mater.* **198**, 282–290 (2011). <https://doi.org/10.1016/j.jhazmat.2011.10.041>
81. Köse, K., Pişkin, B., Aydinol, M.K.: Chemical and structural optimization of ZnCl₂ activated carbons via high temperature CO₂ treatment for EDLC applications. *Int. J. Hydrog. Energy.* **43**(40), 18607–18616 (2018). <https://doi.org/10.1016/j.ijhydene.2018.03.222>
82. Cuhadaroglu, D., Uygun, O.A.: Production and characterization of activated carbon from a bituminous coal by chemical activation. *Afr. J. Biotechnol.* **7**(20), 3703–3710 (2008)
83. Weber, W.J. Jr., Morris, J.C.: Kinetics of adsorption on carbon from solution. *J. Sanit. Eng. Div.* **89**(2), 31–59 (1963). <https://doi.org/10.1061/JSEDA1.0000430>
84. Ahmad, A.A., Hameed, B.H., Ahmad, A.L.: Removal of disperse dye from aqueous solution using waste-derived activated carbon: Optimization study. *J. Hazard. Mater.* **170**(2–3) (2009). 612–619 <https://doi.org/10.1016/j.jhazmat.2009.05.021>
85. Ahmad, M.A., Puad, N.A.A., Bello, O.S.: Kinetic, equilibrium and thermodynamic studies of synthetic dye removal using pomegranate peel activated carbon prepared by microwave-induced KOH activation. *Water Resour. Ind.* **6**, 18–35 (2014). <https://doi.org/10.1016/j.wri.2014.06.002>
86. Hazzaa, R., Hussein, M.: Adsorption of cationic dye from aqueous solution onto activated carbon prepared from olive stones. *Environ. Technol. Innov.* **4**, 36–51 (2015). <https://doi.org/10.1016/j.eti.2015.04.002>
87. Hassan, W., Noureen, S., Mustaqeem, M., Saleh, T.A., Zafar, S.: Efficient adsorbent derived from Haloxylon recurvum plant for the adsorption of acid brown dye: Kinetics, isotherm and thermodynamic optimization. *Surf. Interfaces.* **20**, 100510 (2020). <https://doi.org/10.1016/j.surfin.2020.100510>
88. Sujana, M.G., Pradhan, H.K., Anand, S.: Studies on sorption of some geomaterials for fluoride removal from aqueous solutions. *J. Hazard. Mater.* **161**(1), 120–125 (2009). <https://doi.org/10.1016/j.jhazmat.2008.03.062>

Publisher's Note Springer Nature remains neutral with regard to jurisdictional claims in published maps and institutional affiliations.